

Self-Supervised Uncalibrated Multi-View Video Anonymization in the Operating Room

Keqi Chen^{a,*}, Vinkle Srivastav^{a,b}, Armine Vardazaryan^b, Cindy Rolland^b, Didier Mutter^{b,c}, Nicolas Padoy^{a,b}

^a*University of Strasbourg, CNRS, INSERM, ICube, UMR7357, France*

^b*IHU Strasbourg, 67000 Strasbourg, France*

^c*University Hospital of Strasbourg, 67000 Strasbourg, France*

Privacy preservation is a prerequisite for using video data in Operating Room (OR) research. Effective anonymization relies on the exhaustive localization of every individual; even a single missed detection necessitates extensive manual correction. However, existing approaches face two critical scalability bottlenecks: (1) they usually require manual annotations of each new clinical site for high accuracy; (2) while multi-camera setups have been widely adopted to address single-view ambiguity, camera calibration is typically required whenever cameras are repositioned. To address these problems, we propose a novel self-supervised multi-view video anonymization framework consisting of whole-body person detection and whole-body pose estimation, without annotation or camera calibration. Our core strategy is to enhance the single-view detector by “retrieving” false negatives using temporal and multi-view context, and conducting self-supervised domain adaptation. We first run an off-the-shelf whole-body person detector in each view with a low-score threshold to gather candidate detections. Then, we retrieve the low-score false negatives that exhibit consistency with the high-score detections via tracking and self-supervised uncalibrated multi-view association. These recovered detections serve as pseudo labels to iteratively fine-tune the whole-body detector. Finally, we apply whole-body pose estimation on each detected person, and fine-tune the pose model using its own high-score predictions. Experiments on the 4D-OR dataset of simulated surgeries and our dataset of real surgeries show the effectiveness of our approach achieving over 97% recall. Moreover, we train a real-time whole-body detector using our pseudo labels, achieving comparable performance and highlighting our method’s practical applicability. Code will be available at https://github.com/CAMMA-public/OR_anonymization.

Keywords: **Anonymization, Domain adaptation, Multi-view person association, Operating room, Self-supervised learning**

1. Introduction

The operating room (OR) is a visually complex scene with various medical instruments and multiple clinicians. In recent years, hospitals across various sites have increasingly implemented video recording systems in the ORs with the overarching aim to develop novel context-aware systems [3, 4, 7, 13, 23, 35, 44]. These systems hold significant potential to detect adverse events in real time, optimize clinical workflow processes, facilitate safe human-robot collaboration, and assist in decision-making by automatically analyzing various clinical activities [27, 28, 48, 37]. However, due to the strict ethical regulations such as the Health Insurance Portability and Accountability Act (HIPAA) [1] in the United States and the General Data Protection Regulation (GDPR) [39] in the European Union, video anonymization is required to be applied on the recorded videos before external study in order to protect the privacy of both clinicians and patients. Specifically, it is usually required to blur the eyes, faces or even half bodies of all the persons in the OR. Since each surgery usually takes hours, it is unrealistic to manually anonymize these videos. Although generating low-resolution videos is an easy solution [43], it leads to severe information loss of the holistic

scene. Therefore, it is necessary to develop effective methods towards automatically localizing the persons in the OR for anonymization, in order to advance further OR-related study.

A critical challenge in automatic OR video anonymization is to minimize missed detections, which are also known as false negatives. In practice, even a single missed detection may violate the ethical regulations, and thus a manual review process is strictly required to ensure that every person is properly anonymized through a frame-by-frame inspection. As the false negative rate increases, the time and effort of the review process will be significantly inflated since the reviewer will need to manually blur every neglected person. According to our experiments, although the state-of-the-art approach [16] can anonymize over 92% persons, there would still be more than 20,000 missed detections in a single one-hour video, which would require over 20 hours of manual review assuming that it takes 4 seconds to detect and blur one missed person. Therefore, developing a robust detection framework that minimizes missed detections is essential to ensure the practical scalability of an anonymization pipeline.

With the rapid development of object detection and human pose estimation, most existing works adopt pretrained detectors for OR video anonymization [9, 16]. However, these off-the-shelf detectors suffer from high false negative rates due to the substantial domain gap between the OR and natural im-

*Corresponding author: keqi.chen@unistra.fr

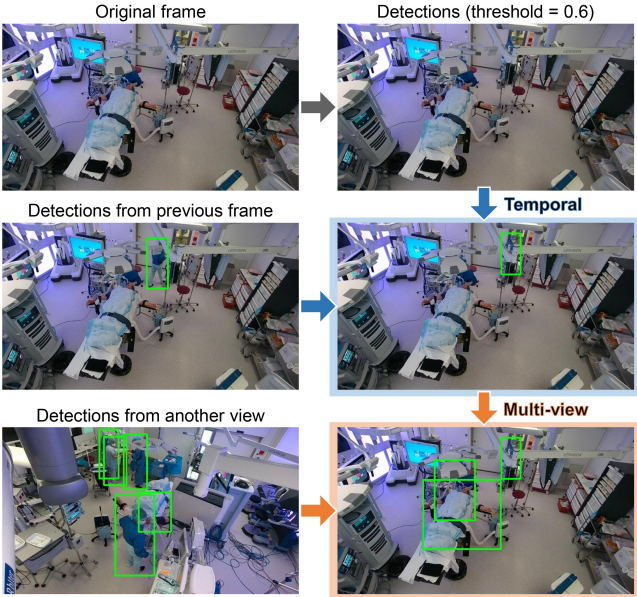


Fig. 1: Examples of robust whole-body detection in the operating room using temporal and multi-view context. In the current frame, the detector fails to detect any instance. Using a tracker and detections from previous frame, we find one clinician; using multi-view person association and detections from another view, we find another clinician and the patient.

ages: clinicians typically wear masks and caps, and medical equipment causes significant occlusion. Although fine-tuning the models on domain-specific data can mitigate the domain gap, scaling such an approach is hindered by two critical bottlenecks. First, obtaining site-specific manual annotations is labor-intensive, and existing public datasets [44, 35] lack the diversity required for generalization. Second, while multi-view analysis [4, 44, 35, 3, 36] resolves single-view ambiguity, it traditionally relies on rigid camera calibration. Existing approaches fail to address these problems simultaneously: Is-senhuth *et al.* [16] pioneer self-supervised domain adaptation using pseudo labels but neglected temporal consistency and multi-view analysis; Bastian *et al.* [3] achieve robustness via 3D point clouds but their work requires calibrated RGB-D setups that increase the deployment complexity. Therefore, developing a framework that is both self-supervised (label-free) and uncalibrated (setup-free) is essential for practical, scalable OR anonymization.

In this work, we propose a *self-supervised uncalibrated multi-view video anonymization* approach, without using any annotations. We hypothesize that combining tracking and multi-view association will effectively reduce false negatives of an off-the-shelf detector through temporal and multi-view consistency. These augmented detections will serve as pseudo labels to allow self-supervised domain adaptation.

Inspired by the observation in [16] that the pose estimation-based approach performs better than face detection for coarse localization, we design a two-stage pipeline, where we first conduct whole-body bounding box detection in the OR to localize all the persons, and then apply whole-body pose estimation for each one of them. This pipeline offers two distinct advantages: (1) it ensures more robust localization in com-

plex OR scenes through whole-body detection, which relies on more abundant features compared to face or visible-body detection; (2) it enables precise, granular anonymization of any desired body region (e.g., eyes, faces, or half bodies) according to different anonymization protocols.

In our pipeline, the anonymization performance is heavily dependent on the recall of the first-stage whole-body detector, and thus we propose to reduce missed detections through tracking and multi-view association. Fig. 1 shows an example of our strategy: in the current frame, the detector fails to detect any person with a high score threshold; based on the detections from previous frame and a motion-based tracker, we find the clinician close to the door; based on the detections from a different view and multi-view person association, we find another clinician and the patient.

Our association strategy is inspired by a tracker named ByteTrack [52], which treats every detection box as a potential association match rather than considering only the high-score ones. Similarly, we extend it to the multi-view scenario. We first use an off-the-shelf whole-body detector to collect a large set of detections using a low-score threshold. Then, we apply ByteTrack [52] in each view to retrieve the low-score boxes by tracking. Subsequently, using these tracked boxes in each view as queries, we train a multi-view association model in a self-supervised way [6], and conduct the association to retrieve the low-score detections in the other views that may have been neglected by tracking due to occlusion. In the end, we have all the retrieved detections as the augmented detections.

To further refine the whole-body detection through domain adaptation, we use these augmented detections as pseudo labels to fine-tune the whole-body detector, and repeat the detection, tracking, and multi-view association steps to generate better pseudo labels iteratively. Our approach also enables real-time applicability as we can train a real-time detector using the generated high-quality pseudo labels. After obtaining the final whole-body detections, we fine-tune the whole-body pose detector using its own high-score joint predictions, which can locate the desired keypoints more accurately.

We evaluate our approach on both the 4D-OR dataset [35] of simulated surgeries and our collected dataset of real surgeries in a more complex scene. For each person, we annotate (1) the whole-body bounding box, (2) the “hard case” flag (over 67% occlusion), and (3) three keypoints (eyes and chin) if they are visible. We also introduce two new metrics to quantify robustness against challenging scenes: (1) hard case recall, which calculates the recall rate of the hard cases; (2) multi-view recall, which measures the percentage of subjects anonymized across all camera views in which they appear. Experimental results show that our approach outperforms existing methods, specifically by achieving a recall rate over 97% on both datasets. Compared to state-of-the-art approaches, ours reduces 13,500 missed detections in a one-hour real surgical video, which saves significant manual reviewing time.

We summarize our contributions as follows: (1) We address video anonymization in the OR without using any annotations. (2) We propose a two-stage anonymization pipeline

that detects whole bodies and estimates whole-body keypoints, which achieves state-of-the-art performance and supports anonymization of any desired body region. (3) We propose to combine tracking and multi-view person association for more robust whole-body detection using temporal and multi-view context. (4) We solve domain adaptation and real-time detection by using spatial-temporally augmented detections as pseudo labels for model fine-tuning. (5) We propose hard case recall and multi-view recall as two new metrics, and evaluate different approaches on both actor-simulated and real surgical videos at three anonymization levels: whole-body, face, and eye.

2. Related work

2.1. Operating room datasets

Despite the growing number of intra-corporeal OR datasets in recent years [32, 30, 22, 5], room-level OR datasets captured by ceiling-mounted cameras remain scarce. Belagiannis *et al.* [4] propose the first multi-view OR dataset named MultiHumanOR, which consists of simulated surgeries with human pose annotations. To introduce data captured during real interventions, Srivastav *et al.* [44] propose the MVOR image dataset, the first multi-view RGB-D dataset with 3d human poses. In order to untangle the interactions between clinicians and objects, Özsoy *et al.* [35] propose the 4D-OR dataset of simulated knee surgeries with semantic scene graph annotations. Then, to enable multi-modal analysis in the OR, they further propose the MM-OR dataset [36], which consists of robotic knee replacement surgeries with a wide range of data sources. With these existing datasets, several computer vision tasks in the OR are supported, such as human pose estimation [12, 43], semantic scene graph generation [33, 38], surgical phase recognition [34], and panoptic segmentation [36]. However, none of these datasets capture real surgical procedures that are much more visually complex. Consequently, they fail to provide the necessary context for addressing missed detections in real-world video anonymization.

2.2. Video anonymization in the operating room

Due to the explosive growth of video data and rising concerns over personal privacy, video anonymization has received growing attention in recent years, where face anonymization plays a significant role [10, 29, 40]. In the OR, anonymizing recorded videos is a critical prerequisite for external studies to protect the identities of both clinicians and patients. Although generating low-resolution videos [43] or using depth videos [17] are feasible solutions in certain scenarios, the inevitable information loss brings severe challenges to the subsequent video analysis. Therefore, face anonymization in the OR becomes an important research area, which relies on accurate face detection. However, the advanced face detection models [31, 14] trained on the WIDER Faces dataset [51] perform poorly in the complex OR scene due to the large domain gap [16]. To address the problem, Flouty *et al.* [9] propose an

OR dataset named FaceOff for model fine-tuning, which contains 6,371 images with face annotations. To implement domain adaptation without annotations, Issenhuth *et al.* [16] propose an iterative self-supervised learning strategy, where they select high-score detections as pseudo labels in each round to fine-tune the face detector iteratively. However, this approach still suffers from the severe occlusion and does not take advantage of temporal context. To address the single-view ambiguity, Bastian *et al.* [3] utilize multi-view RGB-D cameras to do 3d human pose estimation, but it requires accurate camera poses that are hard to obtain. In contrast, our approach utilizes both temporal and multi-view complementary information for better person localization in the OR, without using any annotations or camera calibration.

2.3. Tracking and multi-view person association

Despite the rapid development of image-based object detection, the complexity and occlusions in the OR scene remain significant challenges, leading to high false negative rates. To address this deficiency, it is necessary to integrate additional temporal and multi-view information. Specifically, multi-object tracking can address transient occlusions, while multi-view association can recover objects obscured in one view but visible in the others.

The advanced multi-object trackers are mostly tracking-by-detection, where they use appearance [50] and motion features [20] to associate the detected boxes with the activated tracklets. To enhance robustness against occlusion, ByteTrack [52] proposes a strategy that includes all the detections regardless of scores in the candidate pool, in order to prevent valid targets from being discarded. This approach has since become a widely-adopted paradigm [2, 26, 45]. In our work, we also use a motion-based tracker to retrieve low-score boxes that exhibit temporal consistency with activated tracklets.

Similarly with tracking, multi-view person association aims to associate the detection boxes in synchronized camera views using appearance [49, 11] or geometric features [25, 41]. In order to encode both appearance and geometric features for robust multi-view association without using any annotations or camera calibration, Self-MVA [6] trains a multi-view encoder by distinguishing whether two images from different camera views are captured at the same time. In this work, we optimize Self-MVA to specifically address false negatives: instead of finding associations between high-score boxes, we expand the search space to include all the detected boxes in the other views regardless of scores. This allows us to retrieve the heavily occluded persons if they are visible in the other views.

3. Methodology

3.1. Problem overview

With fixed camera positions in the OR, given multi-view videos of n consecutive RGB frames $\mathcal{V} = \{x_1, x_2, \dots, x_n\}$ where $x_i \in \mathbb{R}^{C \times 3 \times H \times W}$ represents a multi-view image set from C cameras with height H and width W , the goal is to conduct video anonymization by detecting sensitive anatomical regions, such as faces, eyes, and half bodies. To address the problem, we

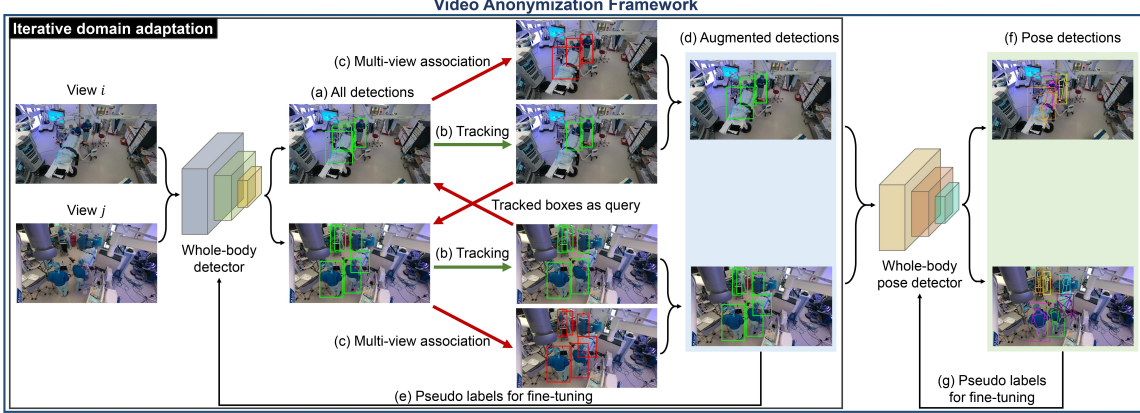


Fig. 2: Framework of our two-stage approach, including whole-body detection and whole-body pose estimation. During training, we apply iterative domain adaptation for whole-body detection: in each round, (a) we use a whole-body detector to generate detections by applying a low-score threshold; (b) we use tracking to obtain tracklets; (c) we use tracklets and multi-view association to find missing detections; (d) we merge tracklets and association results as augmented detections; (e) we fine-tune the detector using augmented detections as pseudo labels. For the whole-body pose detector, we (f) predict poses and (g) fine-tune the model using the high-score predictions on the augmented whole-body detections.

propose a two-stage pipeline, where we first detect the whole bodies using temporal and multi-view context, and then conduct whole-body pose estimation to localize the keypoints.

In the following, we describe our framework as shown in Fig. 2. We first use an off-the-shelf whole-body detector [53] to initially collect a large set of detections in each view with a low-score threshold. Then, to recover false negatives, we formulate both tracking and multi-view association as retrieval tasks: the high-score detections serve as queries, while the complete set of detections in the next frame or in the other views constitutes the candidate pool (referred to as the “gallery”). Specifically, we apply a tracker [52] in each view to obtain all the tracklets. Using these tracklets as queries and all the detected boxes in the other views as the gallery, we conduct multi-view person association by training a geometric encoder in a self-supervised way [6], which further retrieves the false negatives using multi-view geometry. In the end, we have the augmented whole-body detections. In order to implement domain adaptation, we use these augmented detections as pseudo labels, and fine-tune the whole-body detector using OR data. By repeating the previous detection, tracking, and multi-view association steps, we iteratively generate new augmented detections with higher quality, which also supports the training of real-time detectors. Finally, we conduct whole-body pose estimation, and fine-tune the model using its own high-score joint predictions. During inference, we blur the sensitive regions for each person. We introduce each key step in detail as follows.

3.2. Whole-body detection and tracking

In order to circumvent the dependence on the ground-truth data, we first utilize an off-the-shelf detector [53] trained on the CrowdHuman dataset [42] to detect the whole bodies. Compared to face detection or visible-body detection, whole-body detection takes more advantage of the partially visible body features, and possesses the ability to deduce the positions of the whole bodies even when faced with severe occlusion. After applying the whole-body detector on the videos,

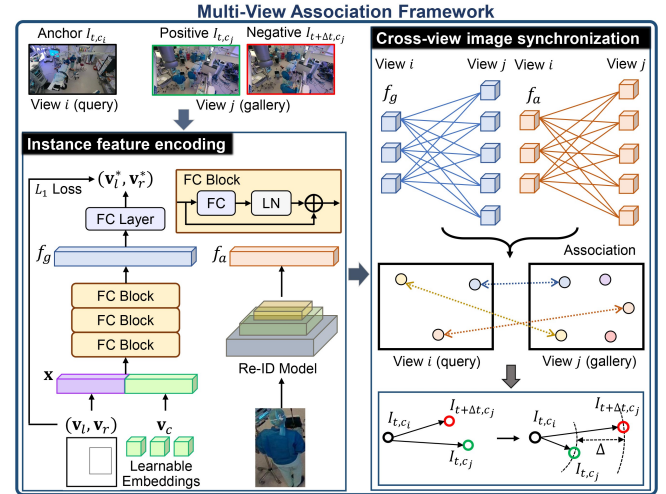


Fig. 3: Framework of the self-supervised multi-view association approach [6] (FC = Fully-Connected, LN = Layer Normalization, Re-ID = Re-IDentification). For each anchor image, we construct a triplet by selecting synchronized and non-synchronized images in a different view. Then, we encode each detected person’s appearance features using a person Re-ID model, map their geometric information to a unified geometric feature space using positional encodings and learnable camera embeddings, and then decode the original 2d position. Finally, we use encoded features to conduct instance association along with triplet-based metric learning. Best viewed in color.

we have all the detected boxes as \mathcal{D} .

Due to the intrinsic domain gap between the OR and natural scenes, the high-score detections tend to ignore the persons that are partially occluded, while the low-score ones contain too many false positives. To retrieve the false negatives using temporal context, we apply ByteTrack [52] for each video. Specifically, we classify all detections \mathcal{D} into high-score set \mathcal{D}^h and low-score set \mathcal{D}^l using a manually-defined threshold. For each timestamp t , we first use the Kalman Filter to predict the locations of the activated tracklets (tracklets successfully associated with prior detections), and then associate them with the high-score boxes \mathcal{D}_t^h , using IoU distances and Hungarian matching [21]. Then, for the unmatched tracklets, we

re-associate them with the low-score boxes \mathcal{D}'_t to find potential false negatives. Lastly, for the remaining high-score boxes, we initialize them as new tracklets; for the tracklets that are not associated for some time, we de-activate them. After processing the videos, we have the tracked boxes as \mathcal{T} , which is a superset of \mathcal{D}^h , as shown in Fig. 2.

3.3. Self-supervised multi-view person association

To further retrieve the false negatives using multi-view geometry, we propose to train a geometric encoder that measures boxes' geometric distances in different views. Inspired by Self-MVA [6], a self-supervised uncalibrated multi-view association approach, we train the encoder via a pretext task, cross-view image synchronization, which aims to distinguish whether two images of different views are captured at the same time. Specifically, we solve this task by encoding instance features and conducting cross-view instance association to compute the image-level distance. Unlike the original Self-MVA that only associates high-score boxes, we expand the search space to include all the detected boxes in the other views regardless of scores. Therefore, the trained encoder is capable of finding geometric associations between high-score and low-score boxes, and thus enables retrieving missed detections. The learning framework is shown in Fig. 3.

For each detected person with normalized top-left and bottom-right corner point positions $(\mathbf{v}_l, \mathbf{v}_r)$, we first map them to a higher dimensional hypersphere [46] as follows, where $\mathbf{b}_j (1 \leq j \leq N)$ are the learnable Fourier basic frequencies:

$$\gamma(\mathbf{v}) = [\sin \mathbf{f}_1, \cos \mathbf{f}_1, \dots, \sin \mathbf{f}_N, \cos \mathbf{f}_N]^T, \quad (1)$$

$$\mathbf{f}_j = 2\pi \mathbf{b}_j^T \mathbf{v}. \quad (2)$$

Then, to encode camera poses, we maintain learnable camera embeddings $\mathbf{v}_c \in \mathbb{R}^{C \times V}$ of size V for C views. For each person, we concatenate its 2d box representation and the camera embedding and pass it through fully-connected (FC) blocks $F(\cdot)$ to obtain the geometric features f_g :

$$\mathbf{x} = [\gamma(\mathbf{v}_l), \gamma(\mathbf{v}_r), \mathbf{v}_c], \quad (3)$$

$$f_g = F(\mathbf{x}). \quad (4)$$

Consequently, for all detections \mathcal{D} , we obtain their geometric features $\mathcal{F}_g = \{f_g^1, \dots, f_g^{|\mathcal{D}|}\}$. Additionally, using an off-the-shelf person re-identification model [54], we obtain the appearance features $\mathcal{F}_a = \{f_a^1, \dots, f_a^{|\mathcal{D}|}\}$.

To compute the overall distance between two images, we apply Hungarian matching to bridge the gap between instance-wise and image-wise distances. Inspired by ByteTrack [52] that associates tracklets with all the boxes regardless of scores, we extend it to multi-view domain, by using tracked boxes \mathcal{T}_t at time t as queries, and using all the detected boxes \mathcal{D}_t as the gallery for association. Specifically, given an anchor image $I_{t,1}$ and another image $I_{t,2}$, we use $\mathcal{T}_{t,1}$ as queries and $\mathcal{D}_{t,2}$ as the gallery. Then, we compute the normalized appearance and geometric Euclidean distance matrix $(\mathcal{E}_a, \mathcal{E}_g) \in \mathbb{R}^{|\mathcal{T}_{t,1}| \times |\mathcal{D}_{t,2}|}$, and take their weighted sum as the overall distance matrix \mathcal{D} , representing instance-wise distances:

$$\mathcal{E} = \alpha \mathcal{E}_a + (1 - \alpha) \mathcal{E}_g. \quad (5)$$

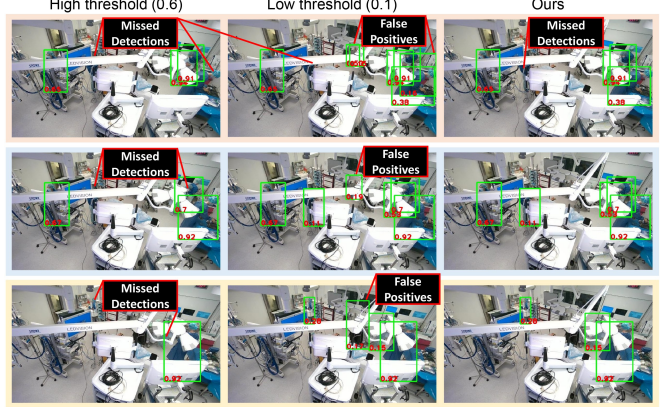


Fig. 4: Comparison of different ways to generate pseudo labels: (1) setting the score threshold to 0.6 will introduce false negatives (missed detections); (2) setting the score threshold to 0.1 will introduce false positives; (3) our strategy combining tracking and multi-view person association obtains pseudo labels of the best quality.

After applying Hungarian matching, we obtain the matched row and column indices $(\mathcal{M}_r, \mathcal{M}_c) \in \mathbb{R}^m$ of matrix \mathcal{E} , where $m = \min(|\mathcal{T}_{t,1}|, |\mathcal{D}_{t,2}|)$. In the end, we average the pairwise instance-wise distances as the image-wise distance \mathcal{H} :

$$\mathcal{H} = \frac{1}{m} \sum \mathcal{E}[\mathcal{M}_r; \mathcal{M}_c]. \quad (6)$$

Finally, we conduct triplet-based metric learning. Given an anchor image I_{t,c_i} from view i at time t , we construct a triplet $(I_{t,c_i}, I_{t,c_j}, I_{t+\Delta t, c_j})$, where (I_{t,c_i}, I_{t,c_j}) is the positive pair, and $(I_{t,c_i}, I_{t+\Delta t, c_j})$ is the negative pair. Δt is randomly chosen that satisfies $\Delta t \in [t_{\min}, t_{\max}]$, where $[t_{\min}, t_{\max}]$ is manually defined frame range. Then we compute the triplet loss L_{syn} for training:

$$L_{\text{syn}} = \max(0, \mathcal{H}_{I_{t,c_i}, I_{t,c_j}} - \mathcal{H}_{I_{t,c_i}, I_{t+\Delta t, c_j}} + \Delta), \quad (7)$$

where Δ is the margin between positive and negative pairs.

To reduce the solution space and stabilize the training, we apply self-supervised multi-view re-projection loss as introduced in [6]. In order to prevent potential information loss during geometric feature encoding, we project f_g back to the original view using a single linear layer, obtaining the estimated bounding boxes $(\mathbf{v}_l^*, \mathbf{v}_r^*)$, as shown in Fig. 3. Then, we use $(\mathbf{v}_l, \mathbf{v}_r)$ as the pseudo labels, and compute the L_1 loss as the re-projection loss L_{pro} :

$$L_{\text{pro}} = \mathcal{L}_1(\mathbf{v}_l^*, \mathbf{v}_l) + \mathcal{L}_1(\mathbf{v}_r^*, \mathbf{v}_r). \quad (8)$$

In general, the final loss function is as follows:

$$L = L_{\text{syn}} + L_{\text{pro}}. \quad (9)$$

During inference, for each multi-view image set $\{I_1, I_2, \dots, I_C\}$, we have tracked boxes $\{\mathcal{T}_1, \mathcal{T}_2, \dots, \mathcal{T}_C\}$ and all the detected boxes $\{\mathcal{D}_1, \mathcal{D}_2, \dots, \mathcal{D}_C\}$. We treat each tracked box in each image as the anchor, and conduct person association with the detected boxes in the remaining $C - 1$ images. Consequently, we obtain the associated

boxes $\{\mathcal{V}_1, \mathcal{V}_2, \dots, \mathcal{V}_C\}$. After merging \mathcal{T} and \mathcal{V} using non-maximum suppression (NMS), we have the temporally and spatially associated boxes \mathcal{A} as the augmented detections:

$$\mathcal{A} = \text{NMS}(\mathcal{T}, \mathcal{V}). \quad (10)$$

3.4. Iterative fine-tuning and real-time testing

By integrating tracking and multi-view person association into the framework, our approach can recover a significant number of false negative detections. These augmented detections not only establish a more robust baseline for anonymization, but can also serve as high-quality pseudo labels for fine-tuning the detector, thereby enabling effective domain adaptation to the challenging OR environment. As shown in Fig. 4, compared to setting different score thresholds, our strategy obtains much better pseudo labels.

During training, we use \mathcal{A} as pseudo labels, along with the CrowdHuman dataset [42], to fine-tune the original detector with data in both OR and natural scenes. After model fine-tuning, we re-conduct the detection, tracking and multi-view association, and generate new augmented detections with higher quality. By repeating the above steps iteratively, we continuously improve the detector and retrieve more persons in the OR. Furthermore, we also use pseudo labels to train a real-time detector [15], which enables real-time testing in real-world applications, with negligible impact on performance.

3.5. Whole-body pose estimation

After obtaining whole-body detections, we apply whole-body pose estimation for each person that detects 133 keypoints, which enables anonymization. To achieve self-supervised domain adaptation, we propose to fine-tune a state-of-the-art model using its own joint predictions, similar to [16]. Specifically, we use an RTMPose model [18] trained on 14 public datasets to estimate initial keypoints of the augmented whole-body detections \mathcal{A} . Then, we only keep the high-score keypoints as the pseudo labels. Finally, we fine-tune the model using the OR data and the COCO-Wholebody dataset [19] simultaneously, which allows better performance.

3.6. Inference pipeline

During inference, we apply the fine-tuned whole-body detector on the OR videos to collect a large set of detections with a low-score threshold. Then, we apply tracking in each view to obtain the tracked boxes. In practice, we conduct tracking in two directions: from start to end and from end to start. Afterwards, we use tracked boxes in each frame as queries to conduct multi-view association, and obtain the associated boxes. By merging the tracked boxes and associated boxes, we obtain the final whole-body detections. Finally, we apply whole-body pose estimation to localize the keypoints.

3.7. Implementation details

We use the PyTorch framework to implement our approach with a single NVIDIA RTX 6000 GPU on the Ubuntu system. For tracking, we define detections with scores greater than 0.6 as the high-score set \mathcal{D}^h . During tracking and multi-view association, we consider detections with scores greater than 0.1 (\mathcal{D}^l) valid for retrieval. We train the geometric encoder for 160 epochs, using the Adam optimizer with an initial learning rate of 1e-4, which decreases to 1e-5 at the 120th epoch. For positional encoding, we set N to 128 in (1), and the camera embedding size V is set to 256. Following previous work [6], the sampling range $[t_{\min}, t_{\max}]$ is set to [5, 20]. The α in (5) is set to 0.5. The Δ in (7) is set to 1.0. For whole-body detection, we fine-tune the detector for 12 epochs in each round, using the AdamW optimizer [24] with an initial learning rate of 2e-4, which decreases to 2e-5 at the 10th epoch. For whole-body pose estimation, we fine-tune the model for 90 epochs, using AdamW optimizer with an initial learning rate of 5e-6, which decreases to 5e-7 at the 50th epoch. We train the real-time whole-body detector for 120 epochs using the AdamW optimizer. NMS threshold in (10) is set to 0.6. We sample frames at 0.1 FPS to fine-tune the whole-body detector (with the entire CrowdHuman dataset) and the pose detector.

4. Experiments

4.1. Datasets and evaluation metrics

We conduct experiments on the 4D-OR [35] and our datasets. 4D-OR records ten simulated knee surgery videos of 1 Frames Per Second (FPS) with six cameras, resulting in a total of 6,734 frames. Our dataset (collected with informed consent from the human participants involved) records five real laparoscopic surgeries of 15 FPS with four cameras, with a total duration of 10.63 hours. For both datasets, we annotate two videos for testing, where each video represents an independent surgery.

The original 4D-OR dataset does not contain facial keypoints or accurate human bounding box annotations. Therefore, we manually annotate the 4D-OR dataset and our dataset: for each person, we annotate (1) the whole-body bounding box, (2) the “hard case” flag (over 67% occlusion), and (3) three keypoints (eyes and chin) if they are visible. In each multi-view image set, we also annotate the identity labels. We annotate the 4D-OR dataset at 0.25 FPS, and annotate our videos at 0.1 FPS. In the end, the 4D-OR test set contains 2,070 images, and ours contains 2,400 images.

We evaluate our approach at three levels: whole-body, face, and eye detection. Since video anonymization does not require precise keypoint localization, we use bounding box-based evaluation metrics for face and eye detection, by manually defining pseudo bounding box labels of a fixed size (40*40 pixels) centered on the ground-truth face and eye locations. Following prior work [16], we use an IoU threshold of 0.3 to determine correct detections. To ensure fair evaluation, when the ground-truth face or eye regions are not visible in a frame due to occlusion or head orientation, the corresponding boxes are excluded from the computation.

Table 1: Comparison with existing approaches on our dataset of real surgeries and 4D-OR dataset of simulated surgeries. We use P-D-DETR as the base detector for self-supervised Iter-Score and our approach. **Best scores**, **second best scores**.

Method	Our dataset of real surgeries													
	Whole body				Face					Eye				
	P	R	AP@.5	R _{hard}	P	R	AP@.3	R _{hard}	MvR	P	R	AP@.3	R _{hard}	MvR
RetinaFace [8]	-	-	-	-	66.30	39.25	31.99	8.91	22.87	65.96	38.87	31.78	8.91	22.62
Head-YOLOv8 [47]	-	-	-	-	33.97	44.82	18.62	12.37	29.56	25.01	33.00	10.99	10.77	21.86
P-D-DETR [53]	65.46	84.57	79.68	64.54	84.38	93.13	88.67	70.21	88.80	85.40	93.17	88.59	70.61	88.86
Iter-Score [16]	95.77	80.61	81.23	52.14	89.51	92.12	88.86	61.97	87.12	89.54	91.99	88.71	62.10	87.00
Ours (P-D-DETR, 8.63 FPS)	85.99	92.56	89.78	85.04	87.58	97.15	88.22	84.44	95.33	88.08	97.06	87.83	84.57	95.21
Ours (DEIM [15], 52.09 FPS)	75.38	91.85	87.80	81.97	86.21	97.55	88.30	86.97	96.06	86.69	97.46	87.82	86.70	95.87

Method	4D-OR dataset of simulated surgeries													
	Whole body				Face					Eye				
	P	R	AP@.5	R _{hard}	P	R	AP@.3	R _{hard}	MvR	P	R	AP@.3	R _{hard}	MvR
RetinaFace [8]	-	-	-	-	77.33	72.01	70.92	54.15	41.86	77.39	71.99	70.91	59.57	42.82
Head-YOLOv8 [47]	-	-	-	-	44.50	51.87	31.07	39.35	18.28	35.06	40.87	20.05	44.04	14.43
P-D-DETR [53]	44.28	87.06	80.40	87.06	73.26	98.54	89.45	97.11	97.25	76.43	97.63	90.11	94.58	96.77
Iter-Score [16]	91.75	80.98	81.16	80.98	82.91	93.45	89.78	70.04	85.91	83.71	93.28	89.89	72.92	86.05
Ours (P-D-DETR, 8.63 FPS)	79.90	90.55	88.41	90.55	82.01	98.64	90.16	96.75	97.18	82.29	97.41	90.30	94.58	96.49
Ours (DEIM [15], 52.09 FPS)	82.68	90.08	88.41	90.08	82.37	98.39	90.15	95.31	97.04	82.93	98.02	90.26	94.95	96.77

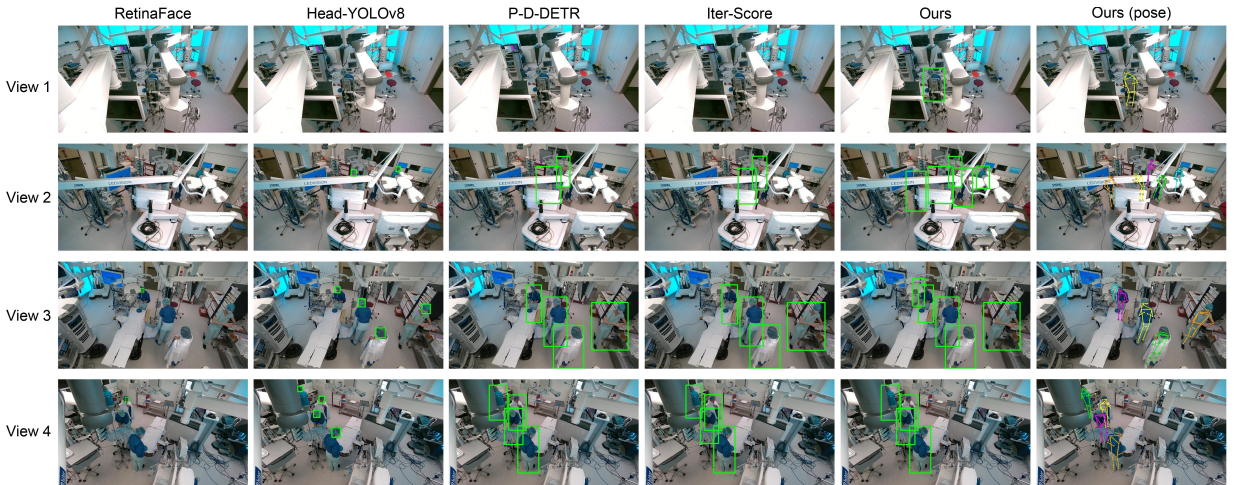


Fig. 5: Examples of different video anonymization approaches on our dataset of real surgeries. (1) RetinaFace [8] fails to detect the faces with masks; (2) Head-YOLOv8 [47] fails to detect the ones with heavily occluded bodies; (3) P-D-DETR [53] (whole-body detection) sets up a strong baseline, but still fails in challenging cases; (4) Iter-Score [16] regresses the bounding boxes more accurately, but fails to retrieve the false negatives; (5) Our approach detects all the persons using temporal and multi-view context, and supports flexible anonymization with human pose estimation.

We evaluate our approach using five metrics: precision (P), recall (R), average precision (AP), hard case recall (R_{hard}), and multi-view recall (MvR). Apart from standard AP, we additionally report P, R, and R_{hard} when the score threshold is set to 0.1, because in the context of video anonymization, R is more important than P in order not to miss a person, and R_{hard} explicitly evaluates models' capability to detect heavily-occluded cases. To further showcase the unique challenges of multi-camera setups, we introduce MvR, a stricter metric that measures the percentage of subjects successfully anonymized across all camera views in which they appear. A subject is only considered correctly anonymized if they are detected in every single view of a given multi-view set.

4.2. Results

We first compare our method with two different types of anonymization approaches: face detection and head detection.

For face detection, we compare with the state-of-the-art RetinaFace model [8] trained on the WIDER FACE dataset [51]. For head detection, we compare with a YOLOv8 model [47] trained on the CrowdHuman dataset [42]. Furthermore, for whole-body detection, we use the Progressive Deformable DETR (P-D-DETR) model [53] trained on the Crowdhuman dataset as the baseline, and compare our approach with a self-supervised detection approach in [16], where we call it Iter-Score. To test the real-time applicability, we train a state-of-the-art real-time detector, DEIM [15], using our generated pseudo labels. For fair comparison, the evaluation strategy of face and eye detection is applied to the outputs of all methods.

Table 1 shows the quantitative results on the 4D-OR and our datasets. Our approach achieves over 97% recall of face and eye detection on both datasets. Compared to face- or head-based approaches, whole body-based ones achieve significantly better performance on both datasets, showing the advantage of whole-body detection in the OR for better lo-

Table 2: Ablation study on tracking and multi-view association augmentation on our dataset of real surgeries. We use the off-the-shelf and fine-tuned whole-body detectors (P-D-DETR) as the baseline. The recall of the baseline is an upper bound of the performance because tracking and multi-view association do not create new boxes. **Best scores**, second best scores.

Method	Whole body				Face					Eye				
	P	R	AP@.5	R _{hard}	P	R	AP@.3	R _{hard}	MvR	P	R	AP@.3	R _{hard}	MvR
Baseline (off-the-shelf)	65.46	84.57	<u>79.68</u>	64.54	83.61	95.20	<u>88.33</u>	75.40	92.15	85.01	94.98	<u>87.79</u>	75.27	91.80
+ tracking	92.06	77.68	72.00	49.04	89.17	92.06	88.25	62.77	87.07	89.52	91.75	87.76	61.44	86.62
+ multi-view association	<u>73.72</u>	<u>83.91</u>	79.79	<u>63.02</u>	85.38	94.82	88.37	73.54	91.51	86.33	<u>94.53</u>	87.81	72.87	91.04
Baseline (fine-tuned)	83.81	92.62	89.75	85.19	87.10	97.19	88.21	84.71	95.46	87.73	97.14	87.82	84.84	95.33
+ tracking	93.55	90.01	89.89	78.58	89.06	96.18	88.24	80.19	93.75	89.38	96.07	87.84	80.05	93.60
+ multi-view association	<u>85.99</u>	<u>92.56</u>	<u>89.78</u>	<u>85.04</u>	<u>87.58</u>	<u>97.15</u>	<u>88.22</u>	<u>84.44</u>	<u>95.33</u>	<u>88.08</u>	<u>97.06</u>	<u>87.83</u>	<u>84.57</u>	<u>95.21</u>

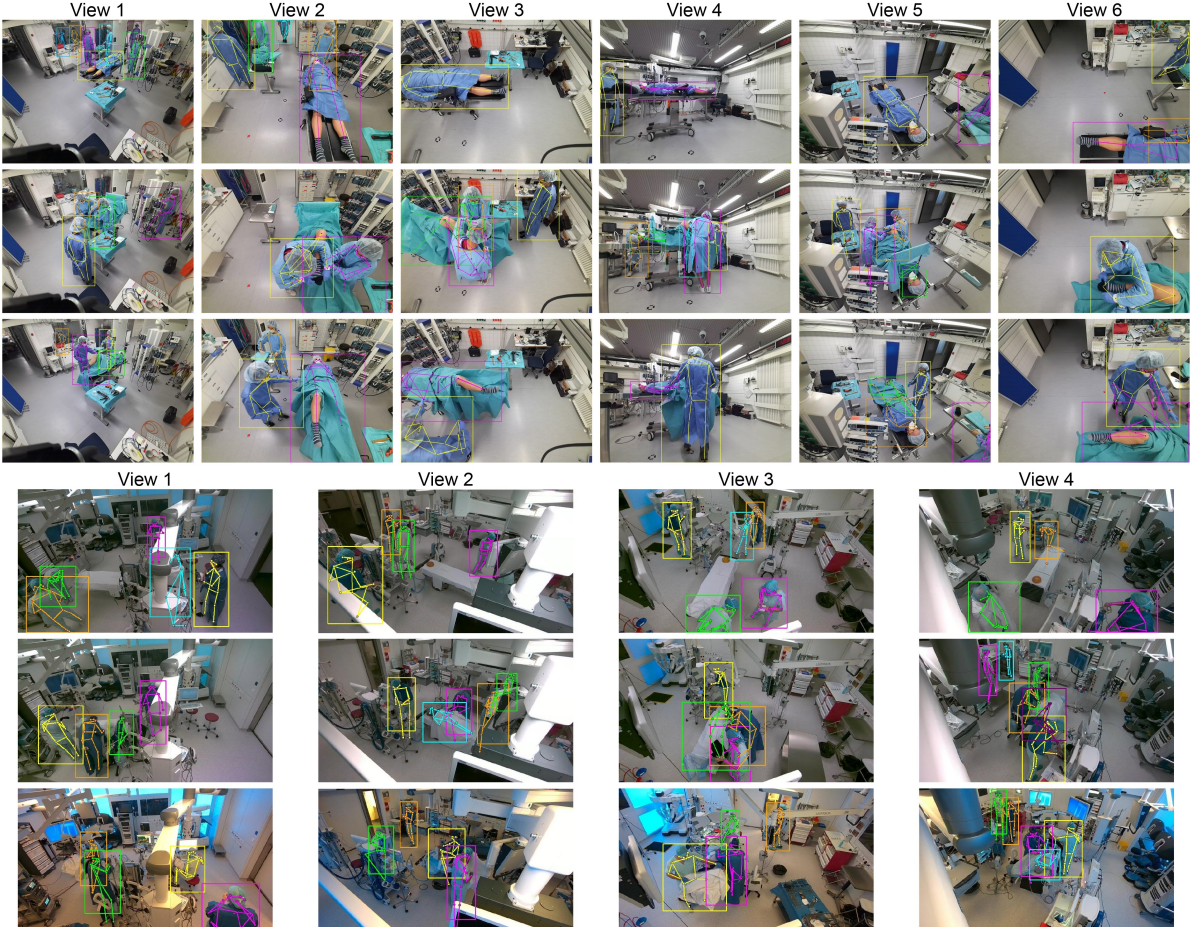


Fig. 6: Qualitative results of our approach on 4D-OR (6 views) and our dataset (4 views) with whole-body bounding boxes and 17-joint poses.

calization. Although Iter-Score [16] is capable of achieving the best precision, it fails to detect hard cases with a low recall rate. In comparison, our approach achieves the best R and R_{hard} on real surgery videos, and the real-time detector trained on our generated pseudo labels achieves a similar performance. It is also noticeable that the performance of all these approaches drops in different degrees when applied to real surgical videos instead of simulated ones (P-D-DETR achieves 98% recall on the 4D-OR dataset, but only 93% on our dataset). This further indicates the importance of studying real OR data, and thus highlights the significance of studying automatic video anonymization. Qualitative examples of different anonymization approaches are shown in Fig. 5. We also display more qualitative results of our approach on the 4D-OR

dataset and our dataset in Fig. 6.

Compared to Iter-Score [16], our approach improves recall by over 5%. Since each video in our dataset is 15 FPS and contains approximately five persons in each frame, our approach reduces 13,500 missed detections in a one-hour video, and thus saves 15 hours of manual review time assuming that it takes 4 seconds to detect and blur a missed person.

4.3. Ablation study

4.3.1. Tracking and multi-view person association

To evaluate the effectiveness of tracking and multi-view association, we conduct an ablation study on our dataset. We set up two sets of experiments using the off-the-shelf and fine-tuned whole-body detectors as the baselines to generate the

Table 3: Ablation study on fine-tuning the P-D-DETR model iteratively on our dataset of real surgeries.

Method	Whole body				Face				Eye					
	P	R	AP@.5	R _{hard}	P	R	AP@.3	R _{hard}	MvR	P	R	AP@.3	R _{hard}	MvR
Baseline	65.46	84.57	79.68	64.54	83.61	95.20	88.33	75.40	92.15	85.01	94.98	87.79	75.27	91.80
1st iteration	82.05	89.42	81.35	75.25	86.56	96.63	88.10	81.25	94.42	87.19	96.48	87.70	80.85	94.16
2nd iteration	83.81	92.62	89.75	85.19	87.10	97.19	88.21	84.71	95.46	87.73	97.14	87.82	84.84	95.33
3rd iteration	74.94	92.22	88.93	84.61	86.69	96.90	88.38	84.57	94.92	87.25	96.74	87.92	84.57	94.64

Table 4: Ablation study on fine-tuning (FT) the whole-body human pose detector using generated pseudo keypoint labels on our dataset of real surgeries.

FT	Face				Eye			
	P	R	R _{hard}	MvR	P	R	R _{hard}	MvR
✗	88.43	94.35	75.66	90.73	88.85	94.42	75.80	90.79
✓	87.58	97.15	84.44	95.33	88.08	97.06	84.57	95.21

candidate pool. Since tracking and multi-view association do not create new boxes, the recall of the baselines represents the theoretical upper bound of the performance, because the baselines use all the boxes in \mathcal{D}^h and \mathcal{D}^l . Results are shown in Table 2. For the off-the-shelf detector, applying tracking significantly boosts precision, but degrades recall dramatically. After adding multi-view association, we achieve a better recall rate close to the upper bound, with much better precision than the baseline. By adopting such a trade-off strategy, our method retrieves the maximum number of true positives with a manageable false positive rate, and thus the final boxes can be used as pseudo labels to fine-tune the detector to retrieve more false negatives. In comparison, fine-tuning only with high-score boxes [16] yields much lower recall, as shown in Table 1.

4.3.2. Iterative whole-body detector fine-tuning

We conduct an ablation study on the iterative training strategy on our dataset. As shown in Table 3, after the first iteration, the detector performs much better with higher precision and recall. After the second iteration, the detector achieves the best performance. After the third iteration, although the detector obtains the highest AP on face and eye detection, the more important recall rate does not get boosted anymore. Therefore, in our dataset of real surgeries, we find that fine-tuning the detector with two iterative rounds is enough for optimal performance.

4.3.3. Fine-tuning whole-body pose detector

To evaluate the effectiveness of fine-tuning whole-body pose detector, we compare the fine-tuned model and the off-the-shelf model by applying them on the final whole-body detections. As shown in Table 4, fine-tuning the model significantly increases the recall rate with a relatively small decrease in precision.

4.4. Limitations

Although our approach achieves remarkable performance in real surgical videos, there are some limitations: (1) if a person is severely occluded in every view for a period of time,

or if it only appears for a few frames, our approach could fail to detect it, making the remaining 3% of persons undetected; (2) multi-view geometry learning requires synchronized camera views with fixed positions; (3) “ghost association” could appear if a person looks too similar with the background. We envision that these constraints could be overcome with more advanced tracking and multi-view geometry techniques in the future.

5. Conclusion

We present a self-supervised approach to address the challenging problem of video anonymization in the operating room (OR). Traditional face detection in the OR suffers from high false negative rates due to severe occlusions from medical equipment and obstruction of facial features by clinicians wearing masks and caps. Therefore, we design a two-stage pipeline that includes whole-body detection and whole-body pose estimation to take advantage of more redundant features against the dramatic domain gap. During the first stage, we utilize tracking and multi-view association to retrieve the missed detections using temporal and multi-view context, and then fine-tune the whole-body detector iteratively using generated pseudo labels. During the second stage, we fine-tune the whole-body pose detector using its own predictions. Experimental results on the 4D-OR dataset of simulated surgeries, as well as on our dataset of real surgeries, demonstrate the effectiveness of the proposed approach by saving 15 hours of manual review time for a single one-hour video. We hope that this work inspires further research that facilitates the collection of more real surgical video recordings across diverse clinical settings, ultimately advancing the development of automated, context-aware support systems in the modern ORs.

6. Acknowledgments

This work was supported by French state funds managed within the Plan Investissements d’Avenir by the ANR under references ANR-22-FA11-0001 (project DAIOR), ANR-10-IAHU-02 (IHU Strasbourg) and by BPI France (Project 5G-OR). This work was also granted access to the servers/HPC resources managed by CAMMA, IHU Strasbourg, Unistra Mesocentre, and GENCI-IDRIS [AD011014722R2, AD011011631R4, and AD011011638R3].

References

[1] Act, A., et al., 1996. Health insurance portability and accountability act of 1996. Public law 104, 191.

[2] Aharon, N., Orfaig, R., Bobrovsky, B.Z., 2022. Bot-sort: Robust associations multi-pedestrian tracking. arXiv preprint arXiv:2206.14651 doi:[10.48550/arXiv.2206.14651](https://doi.org/10.48550/arXiv.2206.14651).

[3] Bastian, L., Wang, T.D., Czempiel, T., Busam, B., Navab, N., 2023. Disguisor: holistic face anonymization for the operating room. International Journal of Computer Assisted Radiology and Surgery 18, 1209–1215. doi:[10.1007/s11548-023-02939-6](https://doi.org/10.1007/s11548-023-02939-6).

[4] Belagiannis, V., Wang, X., Shitrit, H.B.B., Hashimoto, K., Stauder, R., Aoki, Y., Kranzfelder, M., Schneider, A., Fua, P., Ilic, S., et al., 2016. Parsing human skeletons in an operating room. Machine Vision and Applications 27, 1035–1046. doi:[10.1007/s00138-016-0792-4](https://doi.org/10.1007/s00138-016-0792-4).

[5] Che, C., Wang, C., Vercauteren, T., Tsoka, S., Garcia-Peraza-Herrera, L.C., 2025. Surg-3m: A dataset and foundation model for perception in surgical settings. arXiv preprint arXiv:2503.19740 doi:[10.48550/arXiv.2503.19740](https://doi.org/10.48550/arXiv.2503.19740).

[6] Chen, K., Srivastav, V., Mutter, D., Padoy, N., 2025. Learning from synchronization: Self-supervised uncalibrated multi-view person association in challenging scenes, in: Proceedings of the Computer Vision and Pattern Recognition Conference, pp. 24419–24428. doi:[10.1109/CVPR52734.2025.02274](https://doi.org/10.1109/CVPR52734.2025.02274).

[7] Czempiel, T., Sharghi, A., Paschali, M., Navab, N., Moharer, O., 2022. Surgical workflow recognition: from analysis of challenges to architectural study, in: European Conference on Computer Vision, Springer. pp. 556–568. doi:[10.1007/978-3-031-25066-8_32](https://doi.org/10.1007/978-3-031-25066-8_32).

[8] Deng, J., Guo, J., Ververas, E., Kotsia, I., Zafeiriou, S., 2020. Retinaface: Single-shot multi-level face localisation in the wild, in: Proceedings of the IEEE/CVF conference on computer vision and pattern recognition, pp. 5203–5212. doi:[10.1109/CVPR42600.2020.00525](https://doi.org/10.1109/CVPR42600.2020.00525).

[9] Flouty, E., Zisisopoulos, O., Stoyanov, D., 2018. Faceoff: Anonymizing videos in the operating rooms, in: OR 2.0/CARE/CLIP/ISIC@MICCAI. doi:[10.1007/978-3-030-01201-4_4](https://doi.org/10.1007/978-3-030-01201-4_4).

[10] Gafni, O., Wolf, L., Taigman, Y., 2019. Live face de-identification in video, in: Proceedings of the IEEE/CVF International Conference on Computer Vision, pp. 9378–9387. doi:[10.1109/ICCV.2019.00947](https://doi.org/10.1109/ICCV.2019.00947).

[11] Gan, Y., Han, R., Yin, L., Feng, W., Wang, S., 2021. Self-supervised multi-view multi-human association and tracking, in: Proceedings of the 29th ACM international conference on multimedia, pp. 282–290. doi:[10.1145/3474085.3475177](https://doi.org/10.1145/3474085.3475177).

[12] Hansen, L., Siebert, M., Diesel, J., Heinrich, M.P., 2019. Fusing information from multiple 2d depth cameras for 3d human pose estimation in the operating room. International journal of computer assisted radiology and surgery 14, 1871–1879. doi:[10.1007/s11548-019-02044-7](https://doi.org/10.1007/s11548-019-02044-7).

[13] Hu, H., Hachiuma, R., Saito, H., Takatsune, Y., Kajita, H., 2022. Multi-camera multi-person tracking and re-identification in an operating room. Journal of Imaging 8, 219. doi:[10.3390/jimaging8080219](https://doi.org/10.3390/jimaging8080219).

[14] Hu, P., Ramanan, D., 2017. Finding tiny faces, in: Proceedings of the IEEE conference on computer vision and pattern recognition, pp. 951–959. doi:[10.1109/CVPR.2017.166](https://doi.org/10.1109/CVPR.2017.166).

[15] Huang, S., Lu, Z., Cun, X., Yu, Y., Zhou, X., Shen, X., 2025. Deim: Detr with improved matching for fast convergence, in: Proceedings of the Computer Vision and Pattern Recognition Conference, pp. 15162–15171. doi:[10.1109/CVPR52734.2025.01412](https://doi.org/10.1109/CVPR52734.2025.01412).

[16] Issenhuth, T., Srivastav, V., Gangi, A., Padoy, N., 2019. Face detection in the operating room: Comparison of state-of-the-art methods and a self-supervised approach. International journal of computer assisted radiology and surgery 14, 1049–1058. doi:[10.1007/s11548-019-01944-y](https://doi.org/10.1007/s11548-019-01944-y).

[17] Jamal, M.A., Moharer, O., 2022. Multi-modal unsupervised pre-training for surgical operating room workflow analysis, in: International Conference on Medical Image Computing and Computer-Assisted Intervention, Springer. pp. 453–463. doi:[10.1007/978-3-031-16449-1_43](https://doi.org/10.1007/978-3-031-16449-1_43).

[18] Jiang, T., Lu, P., Zhang, L., Ma, N., Han, R., Lyu, C., Li, Y., Chen, K., 2023. Rtmpose: Real-time multi-person pose estimation based on mm-pose. arXiv preprint arXiv:2303.07399 doi:[10.48550/arXiv.2303.07399](https://doi.org/10.48550/arXiv.2303.07399).

[19] Jin, S., Xu, L., Xu, J., Wang, C., Liu, W., Qian, C., Ouyang, W., Luo, P., 2020. Whole-body human pose estimation in the wild, in: European Conference on Computer Vision, Springer. pp. 196–214. doi:[10.1007/978-3-030-58545-7_12](https://doi.org/10.1007/978-3-030-58545-7_12).

[20] Kalman, R.E., 1960. A new approach to linear filtering and prediction problems. Journal of Basic Engineering 82, 35–45. doi:[10.1115/1.3662552](https://doi.org/10.1115/1.3662552).

[21] Kuhn, H.W., 1955. The hungarian method for the assignment problem. Naval research logistics quarterly 2, 83–97. doi:[10.1002/nav.3800020109](https://doi.org/10.1002/nav.3800020109).

[22] Lavanchy, J.L., Ramesh, S., Dall’Alba, D., Gonzalez, C., Fiorini, P., Müller-Stich, B.P., Nett, P.C., Marescaux, J., Mutter, D., Padoy, N., 2024. Challenges in multi-centric generalization: phase and step recognition in roux-en-y gastric bypass surgery. International journal of computer assisted radiology and surgery 19, 2249–2257. doi:[10.1007/s11548-024-03166-3](https://doi.org/10.1007/s11548-024-03166-3).

[23] Li, Z., Shaban, A., Simard, J.G., Rabindran, D., DiMaio, S., Moharer, O., 2020. A robotic 3d perception system for operating room environment awareness. arXiv preprint arXiv:2003.09487 doi:[10.48550/arXiv.2003.09487](https://doi.org/10.48550/arXiv.2003.09487).

[24] Loshchilov, I., Hutter, F., 2017. Decoupled weight decay regularization. arXiv preprint arXiv:1711.05101 doi:[10.48550/arXiv.1711.05101](https://doi.org/10.48550/arXiv.1711.05101).

[25] Luna, E., SanMiguel, J.C., Martínez, J.M., Carballeira, P., 2022. Graph neural networks for cross-camera data association. IEEE Transactions on Circuits and Systems for Video Technology 33, 589–601. doi:[10.1109/TCSVT.2022.3207223](https://doi.org/10.1109/TCSVT.2022.3207223).

[26] Maggiolino, G., Ahmad, A., Cao, J., Kitani, K., 2023. Deep oc-sort: Multi-pedestrian tracking by adaptive re-identification, in: 2023 IEEE International conference on image processing (ICIP), IEEE. pp. 3025–3029. doi:[10.1109/ICIP49359.2023.10222576](https://doi.org/10.1109/ICIP49359.2023.10222576).

[27] Maier-Hein, L., Eisenmann, M., Sarikaya, D., März, K., Collins, T., Malpani, A., Fallert, J., Feussner, H., Giannarou, S., Mascagni, P., et al., 2022. Surgical data science—from concepts toward clinical translation. Medical image analysis 76, 102306. doi:[10.1016/j.media.2021.102306](https://doi.org/10.1016/j.media.2021.102306).

[28] Mascagni, P., Padoy, N., 2021. Or black box and surgical control tower: recording and streaming data and analytics to improve surgical care. Journal of Visceral Surgery 158, S18–S25. doi:[10.1016/j.jviscsurg.2021.01.004](https://doi.org/10.1016/j.jviscsurg.2021.01.004).

[29] Maximov, M., Elezi, I., Leal-Taixé, L., 2020. Ciagan: Conditional identity anonymization generative adversarial networks, in: Proceedings of the IEEE/CVF conference on computer vision and pattern recognition, pp. 5447–5456. doi:[10.1109/CVPR42600.2020.00549](https://doi.org/10.1109/CVPR42600.2020.00549).

[30] Murali, A., Alapatt, D., Mascagni, P., Vardazaryan, A., Garcia, A., Okamoto, N., Costamagna, G., Mutter, D., Marescaux, J., Dallemande, B., et al., 2023. The endoscapes dataset for surgical scene segmentation, object detection, and critical view of safety assessment: Official splits and benchmark. arXiv preprint arXiv:2312.12429 doi:[10.48550/arXiv.2312.12429](https://doi.org/10.48550/arXiv.2312.12429).

[31] Najibi, M., Samangouei, P., Chellappa, R., Davis, L.S., 2017. Ssh: Single stage headless face detector, in: Proceedings of the IEEE international conference on computer vision, pp. 4875–4884. doi:[10.1109/ICCV.2017.522](https://doi.org/10.1109/ICCV.2017.522).

[32] Nwoye, C.I., Yu, T., Sharma, S., Murali, A., Alapatt, D., Vardazaryan, A., Yuan, K., Hajek, J., Reiter, W., Yamlahi, A., et al., 2023. Cholec-triplet2022: Show me a tool and tell me the triplet—an endoscopic vision challenge for surgical action triplet detection. Medical Image Analysis 89, 102888. doi:[10.1016/j.media.2023.102888](https://doi.org/10.1016/j.media.2023.102888).

[33] Özsoy, E., Czempiel, T., Holm, F., Pellegrini, C., Navab, N., 2023. Labrad-or: lightweight memory scene graphs for accurate bimodal reasoning in dynamic operating rooms, in: International Conference on Medical Image Computing and Computer-Assisted Intervention, Springer. pp. 302–311. doi:[10.1007/978-3-031-43996-4_29](https://doi.org/10.1007/978-3-031-43996-4_29).

[34] Özsoy, E., Czempiel, T., Örnek, E.P., Eck, U., Tombari, F., Navab, N., 2024. Holistic or domain modeling: a semantic scene graph approach. International Journal of Computer Assisted Radiology and Surgery 19, 791–799. doi:[10.1007/s11548-023-03022-w](https://doi.org/10.1007/s11548-023-03022-w).

[35] Özsoy, E., Örnek, E.P., Eck, U., Czempiel, T., Tombari, F., Navab, N., 2022. 4d-or: Semantic scene graphs for or domain modeling, in: International Conference on Medical Image Computing and Computer-Assisted Intervention, Springer. pp. 475–485. doi:[10.1007/978-3-031-16449-1_45](https://doi.org/10.1007/978-3-031-16449-1_45).

[36] Özsoy, E., Pellegrini, C., Czempiel, T., Tristram, F., Yuan, K., Bani-Harouni, D., Eck, U., Busam, B., Keicher, M., Navab, N., 2025. Mm-or: A large multimodal operating room dataset for semantic understanding of high-intensity surgical environments, in: Proceedings of the Computer Vision and Pattern Recognition Conference, pp. 19378–19389. doi:[10.1109/CVPR52734.2025.01805](https://doi.org/10.1109/CVPR52734.2025.01805).

[37] Padoy, N., 2019. Machine and deep learning for workflow recognition during surgery. *Minimally Invasive Therapy & Allied Technologies* 28, 82–90. doi:[10.1080/13645706.2019.1584116](https://doi.org/10.1080/13645706.2019.1584116).

[38] Pei, J., Guo, D., Zhang, J., Lin, M., Jin, Y., Heng, P.A., 2024. S²former-or: Single-stage bimodal transformer for scene graph generation in or. *arXiv preprint arXiv:2402.14461* doi:[10.48550/arXiv.2402.14461](https://doi.org/10.48550/arXiv.2402.14461).

[39] Regulation, P., 2018. General data protection regulation. *Intouch* 25, 1–5.

[40] Rosberg, F., Aksoy, E.E., Englund, C., Alonso-Fernandez, F., 2023. Fiva: facial image and video anonymization and anonymization defense, in: *Proceedings of the IEEE/CVF International Conference on Computer Vision Workshops*, pp. 362–371. doi:[10.1109/ICCVW60793.2023.00043](https://doi.org/10.1109/ICCVW60793.2023.00043).

[41] Seo, M., Lee, H.J., Nguyen, X.T., 2023. Vit-p3de*: Vision transformer based multi-camera instance association with pseudo 3d position embeddings., in: *IJCAI*, pp. 1340–1350. doi:[10.24963/ijcai.2023/149](https://doi.org/10.24963/ijcai.2023/149).

[42] Shao, S., Zhao, Z., Li, B., Xiao, T., Yu, G., Zhang, X., Sun, J., 2018. Crowdhuman: A benchmark for detecting human in a crowd. *arXiv preprint arXiv:1805.00123* doi:[10.48550/arXiv.1805.00123](https://doi.org/10.48550/arXiv.1805.00123).

[43] Srivastav, V., Gangi, A., Padoy, N., 2022. Unsupervised domain adaptation for clinician pose estimation and instance segmentation in the operating room. *Medical image analysis* 80, 102525. doi:[10.1016/j.media.2022.102525](https://doi.org/10.1016/j.media.2022.102525).

[44] Srivastav, V., Issenhuth, T., Abdolrahim, K., de Mathelin, M., Gangi, A., Padoy, N., 2018. Mvor: A multi-view rgb-d operating room dataset for 2d and 3d human pose estimation. doi:[10.48550/arXiv.1808.08180](https://doi.org/10.48550/arXiv.1808.08180).

[45] Stanojevic, V.D., Todorovic, B.T., 2024. Boosttrack: Boosting the similarity measure and detection confidence for improved multiple object tracking. *Machine Vision and Applications* 35, 53. doi:[10.1007/s00138-024-01531-5](https://doi.org/10.1007/s00138-024-01531-5).

[46] Tancik, M., Srinivasan, P., Mildenhall, B., Fridovich-Keil, S., Raghavan, N., Singhal, U., Ramamoorthi, R., Barron, J., Ng, R., 2020. Fourier features let networks learn high frequency functions in low dimensional domains. *Advances in neural information processing systems* 33, 7537–7547.

[47] Varghese, R., Sambath, M., 2024. Yolov8: A novel object detection algorithm with enhanced performance and robustness, in: *2024 International Conference on Advances in Data Engineering and Intelligent Computing Systems (ADICS)*, IEEE. pp. 1–6. doi:[10.1109/ADICS58448.2024.10533619](https://doi.org/10.1109/ADICS58448.2024.10533619).

[48] Vercauteren, T., Unberath, M., Padoy, N., Navab, N., 2019. Cai4cai: the rise of contextual artificial intelligence in computer-assisted interventions. *Proceedings of the IEEE* 108, 198–214. doi:[10.1109/JPROC.2019.2946993](https://doi.org/10.1109/JPROC.2019.2946993).

[49] Vo, M., Yumer, E., Sunkavalli, K., Hadap, S., Sheikh, Y., Narasimhan, S.G., 2020. Self-supervised multi-view person association and its applications. *IEEE transactions on pattern analysis and machine intelligence* 43, 2794–2808. doi:[10.1109/TPAMI.2020.2974726](https://doi.org/10.1109/TPAMI.2020.2974726).

[50] Wojke, N., Bewley, A., Paulus, D., 2017. Simple online and realtime tracking with a deep association metric, in: *2017 IEEE international conference on image processing (ICIP)*, IEEE. pp. 3645–3649. doi:[10.1109/ICIP.2017.8296962](https://doi.org/10.1109/ICIP.2017.8296962).

[51] Yang, S., Luo, P., Loy, C.C., Tang, X., 2016. Wider face: A face detection benchmark, in: *Proceedings of the IEEE conference on computer vision and pattern recognition*, pp. 5525–5533. doi:[10.1109/CVPR.2016.596](https://doi.org/10.1109/CVPR.2016.596).

[52] Zhang, Y., Sun, P., Jiang, Y., Yu, D., Weng, F., Yuan, Z., Luo, P., Liu, W., Wang, X., 2022. Bytetrack: Multi-object tracking by associating every detection box, in: *European conference on computer vision*, Springer. pp. 1–21. doi:[10.1007/978-3-031-20047-2_1](https://doi.org/10.1007/978-3-031-20047-2_1).

[53] Zheng, A., Zhang, Y., Zhang, X., Qi, X., Sun, J., 2022. Progressive end-to-end object detection in crowded scenes, in: *Proceedings of the IEEE/CVF conference on computer vision and pattern recognition*, pp. 857–866. doi:[10.1109/CVPR52688.2022.00093](https://doi.org/10.1109/CVPR52688.2022.00093).

[54] Zhou, K., Yang, Y., Cavallaro, A., Xiang, T., 2021. Learning generalisable omni-scale representations for person re-identification. *IEEE transactions on pattern analysis and machine intelligence* 44, 5056–5069. doi:[10.1109/TPAMI.2021.3069237](https://doi.org/10.1109/TPAMI.2021.3069237).